



HAL
open science

The clay fabric of shales is a strain gauge

Tiphaine Boiron, Charles Aubourg, Pierre-Alexandre Grignard, Jean-Paul Callot

► **To cite this version:**

Tiphaine Boiron, Charles Aubourg, Pierre-Alexandre Grignard, Jean-Paul Callot. The clay fabric of shales is a strain gauge. *Journal of Structural Geology*, 2020, 138, pp.104130. 10.1016/j.jsg.2020.104130 . hal-02898124

HAL Id: hal-02898124

<https://hal.science/hal-02898124>

Submitted on 18 Jul 2022

HAL is a multi-disciplinary open access archive for the deposit and dissemination of scientific research documents, whether they are published or not. The documents may come from teaching and research institutions in France or abroad, or from public or private research centers.

L'archive ouverte pluridisciplinaire **HAL**, est destinée au dépôt et à la diffusion de documents scientifiques de niveau recherche, publiés ou non, émanant des établissements d'enseignement et de recherche français ou étrangers, des laboratoires publics ou privés.



Distributed under a Creative Commons Attribution - NonCommercial 4.0 International License

The Clay Fabric of Shales is a Strain Gauge

Tiphaine BOIRON^a, Charles AUBOURG^{b*}, Pierre-Alexandre GRIGNARD^b, Jean-Paul CALLOT^b

^a Université de Pau et des Pays de l'Adour, E2S UPPA, CNRS, DMEX, Pau, France

^b Université de Pau et des Pays de l'Adour, E2S UPPA, CNRS, TOTAL, LFCR, Pau, France.

Corresponding author: charles.aubourg@univ-pau.fr

Key points: (at least three)

Clay, illite, magnetic fabric, cleavage, thrust, Trishear

Abstract

Shales with their large clay fraction are prone to deform in an almost ductile way under tectonic loading. Here, we propose to monitor and quantify the evolution of strained shales clay fabric in the field of illite diagenesis by using magnetic fabric. In the footwall of a south Pyrenean thrust, 281 shales samples have been collected along a 2 km long exceptional exposure. The cleavage evolves from pencil structures at ~1 km of the thrust, to pencil cleavage at ~850 m and slaty cleavage at ~170 m. The average magnetic foliation of illite remains nearly parallel to bedding over a distance of ~600 m despite development of pencil cleavage. It is at ~600 m of the thrust that illite foliation shifts gradually from bedding to cleavage. By contrast, the magnetic fabric scalar data reflect a more continuous evolution of the deformation. The application of a rigid rotation model of the clays allows to quantify the strain magnitude using Eigen values of tensor. This strain magnitude is consistent with distance to the thrust and conforms favorably with a trishear modelling of this thrust damage. We demonstrate therefore that the magnetic fabric of illite-rich shales is a strain gauge.

1. Introduction

Shale formations bear significant economic and engineering interests since they are one of the most abundant rocks in basins (Ma et al., 2018). Shales are important source rocks in the field of both conventional and unconventional petroleum systems. Their low permeability and their ability to heal after a rupture event allows them to secure long-term storage. Thus are they also excellent rocks for CO₂ sequestration (Godec et al., 2013) or for hosting the long-term storage of nuclear waste (Thury and Bossart, 1999). In tectonic environments, shales are potential areas of multiple-scales detachment, and the mechanical properties of these detachments are controlled on a very small scale (Morley et al., 2018). In order to characterize the matrix deformation of shales and to associate a deformation value to them, it is important to characterize the microstructure. Scanning or transmission electron microscopy analysis can account for some characteristics of clay fraction damage (grain rotation or grain kinking) but the small area observed does not provide generally a statistical description of the damage. It would be interesting to be able to access the 3D fabric of a significant fraction of the shales.

The clay fabric of shales has been the subject of numerous studies by X-ray diffraction, goniometry, transmission, and more recently by synchrotron radiation (Haines et al., 2009; Wenk et al., 2019). All these studies have made it possible to properly characterize the clay fraction and its evolution in the context of macroscopic rock damage. Clays are paramagnetic minerals, with strongly anisotropic magnetic properties (Rochette et al., 1992). Clay fabric can therefore be approached using magnetic techniques. In shales, studies have shown that magnetic fabric provides excellent description of the bulk clay fabric in compressive domain (Parés et al., 1999), extensive domain (Cifelli et al., 2004) or in the fault damage zone (Casas-Sainz et al., 2018). The advantage of magnetic fabric with respect to X-ray techniques is that

the volume investigated is of the order of tens of cm^3 , while volume fraction investigated by X-ray is limited to a few mm^3 at most.

In order to be able to follow the evolution of damage to the shale matrix, the study of a deformation gradient in the same formation seems relevant. The Lehigh Gap outcrop in Pennsylvania has been the matter of intense investigation as it displays a strain gradient over ~ 100 m within the monotonous Martinsburg shales (Lee et al., 1986). All stages of cleavage development are represented, from weak cleavage to pencil structure and eventually slaty cleavage. The chlorite and illite fabrics were studied by X-ray diffraction (Hirt et al., 2004; Housen and van der Pluijm, 1990; Lee et al., 1984). Illite fabric mimics quite well the cleavage development from parallel-to-bedding to parallel-to-cleavage. By contrast, chlorite fabric is at 20° oblique to bedding and is parallel-to-cleavage ~ 60 m after the onset of cleavage development. This shift led Lee et al. (1986) to propose that chlorite is reoriented by pressure-solution process and not by rigid-body rotation. Nanoscale observation confirmed that clays evolve by rigid rotation in the pencil cleavage domain and by crystallization dissolution processes in the slaty cleavage domain (Ho et al., 1995; van der Pluijm et al., 1998). Housen et al. (1990; 1991) and Hirt et al. (2004) studied magnetic fabric of Martinsburg shales. Housen et al. (1990) suggested that the magnetic foliation is more consistent with chlorite fabric because of its relative abrupt change from parallel-to-cleavage after ~ 40 m the onset of cleavage. This observation was challenged by Hirt et al. (2004) who measured a more progressive magnetic fabric evolution, more consistent with illite-controlled fabric acquisition. Nevertheless, none of these studies attempted to provide a quantitative correlation between strain and scalar magnetic data, mostly because crystallization dissolution processes have been observed in clays within the slaty cleavage domain, precluding the use of mechanical or geometrical modelling of fabric acquisition. In this study, we present magnetic fabric results of shales from

an exceptional exposure, where the cleavage gradient, exposed along 1 km-long cross section, developed in a shale in which clays are uniformly dominated by illite. Results show an evolution of magnetic fabrics with respect to cleavage development all along the outcrop, consistent with damage induced by thrust propagation.

2. Geological setting and sampling

The studied area, named hereafter the Sigüés section, is located in the southern part of the Pyrenees, in the region of Aragon, Spain (Fig. 1A). This area marks the boundary between the piggy-back turbiditic basin, which rides southward over the deltaic and fluvial clastics sequences along the Jaca thrust (Teixell, 1996). The sedimentary sequence consists in pre-orogenic Triassic marls, sandstones and evaporites (Keuper), covered by late-Cretaceous to Eocene syn-orogenic carbonates and clastics (Labaume et al., 1985). The Mesozoic formation consists in late Cretaceous carbonate shelf (Calcaire des Canyons Fm.) and sandstones (Marboré Fm.). The continental Tremp formation marks the transition between Mesozoic and Cenozoic. It is covered by thick Paleocene carbonates (Ager Fm.). Above, the Arro-Fiscal Fm. (AFF) corresponds to the target area where the strain distribution is studied. The AFF are the lateral equivalent in age to the Hecho turbidites (Eocene), which deposited along E-W through, a few km north of the studied area. The AFF are covered by the Eocene Pampelune shales.

The outcrop is a ~2 km north-south transect, crossing the Sigüés town (Fig. 1A). All information on the dip of the stratification and schistosity comes from our field analysis during sampling. At ~1 km north of Sigüés, the Sierra de Leyre exhibits a stack of three anticlines named hereafter North, Central and South folds. The strike of the folds axes is ~N110, which is also the strike of the cleavage and bedding planes (Fig. 1B). According to Labaume et al. (1985), the North and the Central folds originated from the same ramp (Fig. 1B). By contrast,

the South fold corresponds to a second ramp located farther south. The two ramps originate from a single detachment level within the Triassic. The South fold is limited by a steep emerging thrust (dipping $\sim 60^\circ\text{N}$), which puts abruptly the Marboré and Ager formations over the AFF (Fig. 2). In the hanging-wall, the forelimb is gently dipping to the South ($<10^\circ$). The backlimb is dipping to the North at $\sim 20^\circ$. In the footwall, the AFF displays a well-expressed cleavage fabric, initially reported by Labaume et al. (1985) (fig. 1C). In the following, we will measure the N-S distance from the location of sample 3S1 (N42°38'30.20", W1° 0'43.50", Table) which is at ~ 5 m from the emergent thrust of the South Fold. At $x < 41$ m, bedding displays a tight decametric overturned footwall syncline which parallels the thrust and the cleavage (Fig. 1C). For $x > 41$ m, the bedding of the AFF from the footwall is slightly dipping to the south ($<15^\circ$). A metric fracture network, with both longitudinal (EW) and transversal (NS) fracture is present all along the 2 km long outcrop (Fig. 3A-C) (Crognier et al., 2018).

At $x=2$ km, the outcrop is cleavage-free (fig. 3A). Some pencil structures are observed at $x\sim 1$ km. The onset of incipient pencil cleavage is located at $x\sim 865$ m (Fig. 3B). It is marked by the development of discrete planes dipping to the north ($\sim 30^\circ\text{N}$). The spacing of cleavage plane reaches ~ 5 planes/meter at most (Fig. 3C). For $440 < x < 600$ m, the dip of cleavage ranges from $\sim 30^\circ$ to $\sim 50^\circ$, controlled by the stiffness of the layers. The spacing of cleavage is reducing drastically, reaching the centimeter. Bedding is still observable. For $x < 200$ m, the dip of cleavage ranges between $\sim 60^\circ$ to $\sim 90^\circ$ and the spacing of cleavage is $< 100 \mu\text{m}$ (Fig. 3D). This is the domain of slaty cleavage, in which the bedding is almost completely overprinted by the cleavage (Fig. 3D). The cleavage development is here illustrated by both intensification and steepening when approaching the emergent steep thrust. This is consistent with the initial cross section proposed by Labaume et al. (1985) who reported a close match between thrusts and cleavage development in the Sierra de Leyre. Izquierdo-Llavall et al. (2013) investigated

the cleavage front in this area and proposed that the cleavage development is correlated to the peak burial temperature, $>140^{\circ}\text{C}$. This was confirmed by additional paleothermal values provided by Crognier et al. (2018), where the upper limit of peak burial temperature in AFF is $<200^{\circ}\text{C}$.

A total of 281 oriented standard cores (25 mm diameter, 21 mm height) have been sampled all along the ~ 2 km cross-section (Table in supplementary material). Several zones have been defined, in which we distinguish 37 sub-groups (number of cores comprised between 22 and 5). At $x \sim 2$ km ($n=17$ cores), is our reference of cleavage-free zone. Two sub-groups are defined in that zone (site 1 and 2, Table). Between ~ 2 km and ~ 1 km, the AFF are monotonous, without evidence of pencil structures development. At $1000 < x < 830$ m ($n=86$ cores), the pencil cleavage is gradually developed within ~ 170 m, from few discrete planes to centimetric spacing planes. Fourteen sub-groups are defined along that zone (sites 3-16, Table). For nearly 200 m (800 to 600 m from the fault), rock outcrop conditions prevented adequate sampling. At $597 < x < 444$ m ($n=67$ cores), the pencil cleavage present a centimetric spacing. Nine sub-groups are defined (sites 17-25, Table). For nearly 200 m (400 to 200 m from the fault), no rock exposure is accessible from the road. At $171 < x < 0$ m ($n=112$ cores), slaty cleavage presents an infra millimetric spacing. Twelve sub-groups are here defined (sites 26-37, Table), among which 5 (sites 33-37, Table) are within the footwall syncline which shows with overturned bedding.

3. Methods

The anisotropy of low-field magnetic susceptibility (AMS) has proven to be a powerful technique to study shale fabrics (Parés, 2015). Its success is due to the rapidity of measurement (few minutes) of a reasonable volume of material ($\sim 10 \text{ cm}^3$), and its sensitivity (Hrouda et al., 1997). AMS is described satisfactorily with a symmetric tensor which Eigen

values are $K_1 \geq K_2 \geq K_3$. The resolution of the tensor provides a statistical description. Each axis is then associated with a confidence ellipse at 95% level. In sedimentary rocks, it is common to use the magnetic foliation plane (K_1 - K_2 plane, K_3 as pole) and the magnetic lineation (K_1) as structural elements. This can be compared to sedimentary and structural planes and lineations that are commonly observed in the field. In strained shales from compressional basin, the magnetic foliation is generally parallel to the bedding plane and the magnetic lineation lies perpendicular to the layer parallel shortening axis (Aubourg et al., 2004; Robion et al., 2007; Weil and Yonkee, 2012).

The mean magnetic susceptibility K_m is a proxy of the content of magnetic particles ($K_m = (K_1 + K_2 + K_3)/3$). The shape of AMS ellipsoid is commonly described by the corrected degree of anisotropy P_j ($P_j = K_1/K_3)^a$, with $a = \sqrt{1 + \frac{T^2}{3}}$ and the shape parameter T ($T = (\ln(K_2/K_3) - \ln(K_1/K_2))/(\ln(K_2/K_3) + \ln(K_1/K_2))$). T ranges from -1 (prolate shape ellipsoid) to +1 (oblate shape ellipsoid) (Hrouda et al., 1997). From the 37 sub-groups, we calculate tensorial mean (Jelínek and Kropáček, 1978). The MFK1-FA (Agico®) was used for all measurements (frequency 976 Hz, magnetic field 200 A/m, sensitivity 2×10^{-8} SI).

To investigate rock magnetic properties, we ran hysteresis loop measurements on Vibrating Sample Magnetometer (Princeton) and low-temperature monitoring of artificial remanence on Magnetic Properties Measurement System (Quantum Design) housed at the Institute of Rock Magnetism (Minneapolis, USA). In both settings, we crushed manually powder from shales and put ~ 0.5 g of this powder in gel caps. We performed X-ray diffraction on rock powder at XRD/XRF service-GET Laboratory (Toulouse, France).

4. Rock magnetism of AFF

The low-field magnetic susceptibility is homogenous all along the section, with K_m ranging from 68 to 165 μSI (mean value of $K_m=105\pm 15 \mu\text{SI}$). The hysteresis loop measurements of induced magnetization on 12 samples reveal a systematic linear trend (Fig. 4A), indicating that magnetic susceptibility is strongly governed by paramagnetic minerals. The high-field magnetic susceptibility (derived from slope correction of hysteresis loops) is ranging from 61 to 132 μSI . It turns out that the ferromagnetic contribution is very low (Fig. 4B), evidencing a very soft coercive ferromagnetic mineral. To elucidate the origin of ferromagnetic mineral, we investigate the magnetic transition at low temperature of representative shales following Aubourg and Pozzi (2010) protocol. A room-temperature isothermal remanent magnetization (RT-SIRM) was imparted at 2.5 Tesla. The monitoring of cooling and warming RT-SIRM was performed using a MPMS in the range 300-20K. An induced magnetic field of 5 mT was imparted upward to track the evolution of induced magnetization. The remanence of RT-SIRM is low of the order of $10^{-4} \text{ Am}^2/\text{kg}$ (Fig. 4C). A non-reversible Verwey transition is observed at $\sim 120\text{K}$ (Fig. 4C), which is indicative of stoichiometric magnetite (Özdemir et al., 1993). An induced magnetization is observed below $\sim 80\text{K}$. This comportment was named P-behavior by Kars et al. (2011) and it is presumably representative of superparamagnetic ferromagnetic particles.

X-ray diffraction analysis have been performed on 11 samples, spanning over the 2 km transect (Fig. 5). All spectrums are similar, indicating no significant variation in mineralogy with distance to the thrust. Clays are dominated by well crystallized illite and few biotites and chlorites. This is consistent with Izquierdo-Llavall et al. (2013) who reported illite/smectite ratio of 87% in the same area. The clays represent 15-33 % of minerals content. Quartz and calcite represent 29-37% and 30-50% respectively. Only clays have paramagnetic input, while quartz and calcite are essentially diamagnetic ($\sim 10 \mu\text{SI}$) (Rochette et al., 1992). Hence, illites

are the main contributor to the magnetic susceptibility in AFF. Scanning electronic microscope shows the organization of clays within the matrix (Fig. 6). At $x \sim 2$ km from thrust, illite are parallel to bedding. At $x \sim 60$ m, patches of illite are observed. Some illites parallel the cleavage, and some mimic bedding.

5. Magnetic fabric results

We present directional data of anisotropy of AMS in five domains. Overall, when considering the confidence ellipses of each axes (Fig. 7), it appears that K3 axes are better grouped than K1 axes. Within the five domains, the average magnetic lineation (K1m) resulting from tensorial mean is sub-horizontal, trending N110°. This direction is parallel to the fold axis. In the cleavage-free zone ($x > 1$ km) (Fig. 7A), K3 axes are well resolved. The average magnetic foliation (K3m is the average pole) parallels the bedding plane. In the initiation of pencil cleavage area ($1000 < x < 830$ m), where cleavage evolves from metric to decametric spacing (Fig. 7B), the magnetic fabric is similar to the one observed in the zone without cleavage. The magnetic foliation is parallel to bedding despite the development of pencil cleavage. In the pencil cleavage zone ($598 < x < 444$ m), where the spacing of the cleavage is decametric to centimetric, the magnetic fabric evolves differently (Fig. 7C). The individual confidence ellipses of the K3 axes are larger, with major axes pointing in the N-S direction. K3 axes are distributed parallel to poles of bedding and cleavage. Despite this girdle-shaped distribution, the average pole of magnetic foliation is close to pole of bedding. In the slaty cleavage zone, where cleavage spacing is < 100 μm and bedding is horizontal ($171 < x < 44$ m), K3 axes display also large confidence ellipses (Fig. 7D). The pole of magnetic foliation is lying between the pole of bedding and the pole of cleavage. Where bedding is overturned ($x < 44$ m), K3 axes are better defined (Fig. 7E). There is a good match between bedding, cleavage and magnetic foliations.

The corrected degree of anisotropy P_j and the shape parameter T display trends with respect to the distance of the thrust. The mean values of the subgroups (Table) and their 95% standard deviation are considered here (Fig. 8). We observed a general decrease of P_j from the cleavage-free zone ($P_j \sim 1.10$) to the slaty cleavage zone at $x \sim 68$ m ($P_j \sim 1.04$) (Fig. 8A). Then, in the remaining ~ 68 m, P_j increases up to ~ 1.12 . It is worth noting that P_j starts increasing before the development of the footwall syncline. This suggests a sudden and strong reorganization of the illite particle orientation while bedding is still horizontal. The shape parameter T displays a rough 'V' shape from oblate-to-prolate and from prolate-to-oblate (Fig. 8B). In the cleavage-free zone, the AMS ellipsoid is strongly oblate. In the pencil-cleavage domain, a decrease of T is observed from strongly oblate to prolate ($T \sim -0.6$). In the slaty cleavage domain, an increase of T is noticeable with some exception at $x \sim 68$ m where ellipsoid is still prolate. Note that T is strongly oblate in the northern part of slaty cleavage where bedding is horizontal ($52 \text{ m} > x > 44 \text{ m}$). This change is correlated with the increase in the degree of anisotropy P_j .

6. Discussion

6.1. Magnetic mineralogy

Rock magnetism investigation of AFF shows that the magnetic susceptibility is essentially paramagnetic with very little ferromagnetic contribution (Fig. 4A). This observation has been previously reported by Pueyo-Anchuela et al. (2010) in the AFF from the same area. The observation of the Verwey transition at $\sim 120\text{K}$ indicates that stoichiometric magnetite represents the ferrimagnetic phase (Fig. 4C). In addition, we report the presence of fine-grained magnetic particles, as revealed by the presence of P-behavior (Fig. 4C). This magnetic assemblage constituted of stoichiometric magnetite and fine-grained ferromagnetic particles is diagnostic of moderately buried shales according to several studies (Kars et al., 2015). More

precisely, Aubourg et al. (2019) reported a similar pattern of magnetite content through progressive burial of shales. From peak burial temperatures ranging from $\sim 50^{\circ}\text{C}$ to $\sim 350^{\circ}\text{C}$, the content of magnetite evolves from tens of ppm to a few ppm. Sticking to this semi-quantitative calibration, the magnitude of isothermal remanence at saturation of the AFF (RT-SIRM $\sim 10^{-4}$ Am/kg²) is consistent with burial temperatures ranging from 150° to 250°C . This agrees with Izquierdo et al. (2013) and Crognier et al. (2018) burial data, in the $160\text{-}200^{\circ}\text{C}$ range. This moderate burial leads to the formation of authigenic illite at the expense of smectite (Izquierdo et al., 2013). X-ray diffraction analysis of representative samples across the strain gradient area revealed that illite is effectively the major contribution to clays in the AFF (Fig. 5). It is worth noting that we do not see any difference between X-ray diffraction data from cleavage-free samples and strongly deformed ones. This suggests that the growth of clays, if any, is limited to the approach to areas close to the thrust. Therefore, the low-field magnetic susceptibility of the AFF is almost entirely governed by illite. It turns out that magnetic fabric measured by the AMS provides the bulk fabric of billions of illite grains dispersed in the matrix (Fig. 6).

6.2. Magnetic fabric directional data

The directional AMS data of the AFF are at first glance conformable to magnetic fabrics reported in strained shales (Parés, 2015), and more specifically to the magnetic fabrics reported by Pueyo Anchuela et al. (2010) in the North of the Jaca Basin. In the following, we propose a comparison between a schematic 3-step evolution during layer parallel shearing proposed by Parés (2015), our data and Hirt et al. (2004) data from Lehigh Gap (Fig. 9). The Lehigh Gap is, to date, the best example of documented layer parallel shearing in shales. Hirt et al. (2004) AMS data have been measured with the same AF magnetic field (200 A/m) that we used in this study.

Parés (2015) proposed to schematize the evolution of the magnetic fabric of strained shales following 3 steps (Fig. 9A). At Sigüés, a schematic 4-step magnetic fabric is hereafter proposed. Sigüés data are schematized within the same reference frame of Parés (2015) with top-to-the-left shearing (Fig. 9B). We remove from this analysis the samples from the footwall syncline as the bedding and cleavage parallel each other. At Lehigh-Gap, Hirt et al. (2004) proposed a 4-step evolution. From their dataset, we plot a schematic stereographic projection of AMS data with bedding plane restored at horizontal, and application of a rotation along a vertical axis to conform with a top-to-the-left simple shear (Fig. 9C).

The magnetic lineation develops perpendicular to the main shear direction in the cleavage-free domain as well as in the pencil cleavage domain. It should be noted, however, that some K1 axes to Sigüés (Fig. 7D-E) and all K1 axes to Lehigh Gap are arranged parallel to the shearing direction in the slaty cleavage zone. This contrasts with the third step of Parés (2015) model (Fig. 9A). The magnetic foliation at Sigüés is parallel to the bedding within the cleavage-free domain. At Lehigh-Gap, however, the K3 axes are distributed as a small girdle. This results from a competition between the chlorite fabric, oblique to bedding, and the illite/biotite fabric, parallel to bedding (Housen and van der Pluijm, 1990). The intermediate stage of evolution of Parés (2015) suggests that K3 axes shift gradually from the pole of bedding to the pole of cleavage, forming a distinctive girdle (Fig. 9A). Our results at Sigüés conform with Parés (2015) evolution for the cm-spacing area of pencil cleavage (Fig. 9B, 7C). Both extent and location of girdles are consistent with the top-to-the-left shear. However, our results do not conform within the decimetric-spacing pencil cleavage zone (Fig. 9B). No girdling is observed, and each K3 axis is well defined and perpendicular to bedding (Fig. 7B). At Lehigh Gap, the K3 axes display a large girdle between the pole of bedding and the pole of

cleavage both in the domain of pencil structures and the weak cleavage zone. This evolution agrees better with Parés (2015) model, although chlorite fabric obscures the illite fabric.

In the late stage of the 3-step evolution of Parés (2015) model, the magnetic foliation is parallel to the cleavage. At Sigüés, there is a spread of K3 axes between the pole of bedding and the pole of cleavage. The mean magnetic foliation is defined between bedding and cleavage (Fig. 9B, 7D). The lack of good match between K3 axes and pole of cleavage is relatively unexpected. Hirt et al. (2004) observed such obliquity within their domain of weak cleavage and attributed this to a large spreading of 001 illite axes. At Sigüés, SEM inspection comforts this hypothesis because patches of illite parallel to bedding planes, and patches controlled by 40 μm -spaced cleavage are observed (Fig. 6B). In summary, Sigüés data display expected evolution of magnetic fabric of layer parallel shearing, with a significant ~ 200 m offset between the development of pencil cleavage and the girdling of K3.

6.3. *Magnetic fabric scalar data*

At Sigüés, the AMS scalar data evolve with respect to cleavage development. The parameter P_j (Fig. 8A) decreased monotonously (~ 1.10 to ~ 1.04) when approaching the thrust, except near the hinge of the footwall syncline, where a marked increase is observed. As magnetic mineralogy is monotonous all along the outcrop, the decrease in P_j would indicate a progressive disorganization of illite particles, and a quite reorganization of illite near the hinge of the footwall syncline. The shape parameter T displays an oblate-prolate-oblate path (Fig. 8B). The evolution of shape parameter T at Sigüés outcrop is particularly remarkable in the pencil cleavage domain. While the initiation of pencil cleavage begins at ~ 1 km, the T parameter starts to decrease significantly at ~ 840 m from the thrust. At this distance, the magnetic foliation remains controlled by the bedding. It is thus suggested that the T

parameter might be a sensitive parameter to monitor the damage of the matrix. This is in line with observations made by Humbert et al. (2014) and Parés (2015).

To compare Sigüés data to Lehigh Gap data, we have computed the corrected degree of anisotropy P_j and the shape parameter T from the magnetic fabric dataset of Housen et al. (1990) (data are not shown). At Lehigh Gap, P_j decreases from ~ 1.16 (cleavage free) to ~ 1.04 (slaty cleavage). The magnitude of this decrease is comparable to the decrease of P_j observed at Sigüés outcrop (Fig. 8A). The shape parameter T decreases quite regularly at Lehigh Gap from 0.7 (cleavage free) to -0.3 (slaty cleavage). From this comparison, we can say that there are similarities between the Sigüés and the Lehigh-Gap outcrops. However, at Lehigh Gap, no increase of P_j is observed in the most deformed shales.

6.4. Toward a strain quantification

We propose to approximate the strain at Sigüés using Eigen values of AMS as proposed by Humbert et al. (2014). Assuming the magnetic fabric is solely controlled by mechanical processes involving grain rotations and porosity reduction, its evolution can be approached using the March's model of grain rotation (March, 1932). Humbert et al. (2014) estimated horizontal strain of clay-rich sedimentary rocks by using the normalized eigenvalues of the AMS tensor. Three conditions are necessary to apply this method: (1) the main carrier of AMS must be paramagnetic, (2) the platelets must respond to the horizontal strain by crenulation, and (3) there shall not be any change in the mineralogical content (no cementation, dissolution, nor diagenetic replacement). The first condition is fulfilled for the AFF, as shown by the strong paramagnetic behavior of magnetic susceptibility (Fig. 4A) and the similar clay content measured in representative samples (Fig. 5). The second condition is quite probable as we never observed any crystallographic strain evidence, such as twinning or intra grain fractures. The third condition is questionable if clay formation occurred (van der Pluijm et al.,

1998). Formation of new minerals along the cleavage plane is probably a minor process in the AFF because X-ray diffraction patterns are similar in all samples measured along the section (Fig. 5). We therefore consider Humbert et al (2014) model as being relevant to our AMS dataset. This model has been initially developed for lateral shortening but according to Hooyer and Iverson (2000), the clast rotation occurs in a quite similar way in pure and simple shear. To use this model, we distinguish two end members: (1) K3 axes are vertical away from the fault for $x > 440$ m, and (2) K2 axes are vertical near the fault for $x < 440$ m. In the latest, the magnetic foliation parallels the cleavage plane. We assume that the minimum value of T corresponds to the shift between the two end-member geometries, i.e. K3 axes-vertical to K2-axes vertical. There are therefore two equations relating the horizontal strain dl/l to the AMS eigenvalues: $dl/l = 1 - \sqrt{((K1 - K3)/(3(K1 - 1)))}$ for $x > 440$ m, and $dl/l = 1 - \sqrt{((K1 - K2)/(3(K1 - 1)))}$ for $x < 440$ m. Taking the mean values of eigenvalues from tensorial means of the 32 subgroups, we obtain a horizontal strain ranging from 0.02 up 0.76 near the fault (Fig. 8C). We removed from this analysis the sub-groups 33 to 37 at $x < 43$ m, because bedding and cleavage planes are here parallel. The evolution of dl/l fits with a power-law regression $dl/l = 49.425 * \text{distance}^{-0.973}$ ($R^2 = 0.77$). According to this strain approximation, the cleavage-free domain shows $\sim 5\%$ ($dl/l = 0.05$) of shortening. The pencil-cleavage domain is consistent with a shortening ranging from a few percent to $\sim 25\%$. Finally, the slaty-cleavage domain evolves from $\sim 40\%$ to $\sim 75\%$ shortening. This high calculated strain is comforted by the observation of cleavage which overprints almost completely the bedding (Fig. 3D). This is also consistent with reported strain values in slaty cleavage where shortening in excess of 50% is commonly observed (Kisch, 1991).

6.5. *Trishear modeling*

At Lehigh Gap, the origin of the cleavage gradient remains unclear. It is generally considered that a thick conglomerate layer acts as a pressure 'shadow' against cleavage formation in the shales (Holeywell and Tullis, 1975). At Sigüés, we have the chance to observe a relationship between cleavage gradient and exposure of a thrust. To explain both the power-law trend of calculated strains and the kilometric extension of strained shales, we propose to use a trishear modeling of the South Fold, hypothesizing that thrust propagation is accompanied with significant strain in the footwall. Erslev (1991) introduced the concept of triangular zone of deformation –named trishear- at the tip of propagating fault. The basic idea of trishear model is the existence of triangle zone of differential velocity at the tip of the propagating thrust. At the top of this triangle zone, the slip vectors in the footwall are equal to that of the hanging wall, whereas at the base, the slip is zero. The simple shear imposes a footwall syncline geometry that mimic field observations (Hardy & Allmendinger, 2011). Cardoso et al. (2005) have suggested that trishear model works better in homogenous materials but fails with lithology presenting contrasted mechanical behaviors, as these are rather prone to kink banding. In the trishear model, the ratio between the propagation length and the slip along the fault (P/S) and the angle of the trishear zone (the apical angle) both control the distribution of the shear strain recorded in sediments from the footwall (Hardy and Allmendinger, 2011). Potentially, the damage zone is as large as the thrust displacement (Cardozo et al., 2005).

We use FaultFoldForward (FFF) software which is based on algorithms proposed by Allmendinger (1998) and Zehnder and Allmendinger (2000). Several parameters control the trishear model: the dip of thrust, the P/S ratio, the apical angle, and the shortening ratio (Hardy and Allmendinger, 2011). We fit the parameters according to (1) the steep attitude of

emergent thrust marked by the abrupt termination of Ager carbonate layer against the AFF, (2) the 20°S dip of the back limb which parallels theoretically the ramp at depth, and (3) the limited extent of the plateau of Ager Formation (~500 m) (Fig. 1A). Our best model (Fig. 10A) has an apical angle of 110°, a P/S ratio of 1, and a shortening of 1.5 km. The geometry of folded Ager carbonates is respected (Fig. 1B, 2), including the dip of the back limb, the short length of the plateau, and the presence of footwall syncline. Theoretical strain ellipses are provided by the FFF software and the ratio d_l/l is calculated (Fig. 10B). Two observations are striking: 1) the trishear strain is 80% near the thrust and presents large values at 2 km distance (40%). This suggests that a km-large strain domain potentially develops in the footwall of the thrust; 2) the trishear strain displays a power-law trend, which is also consistent with the strain calculated from magnetic fabrics (Fig.8C). Of course, the use of the trishear model is simplistic and it is not possible to compare directly the predicted strain values with the magnetic fabric data. However, this first approach provides a good explanation of both the kilometeric-large extent of strain and the evolution of the power law of strain when approaching the thrust. If the model of trishear can be applied, it is worth noting that the emerged thrust is a part of the upper triangle zone, where intense shear occurred. The main ramp itself remains at depth.

7. Conclusion

At the Sigüés outcrop, a remarkable 1 km-long outcrop allows to monitor all steps of cleavage development in the Arro-Fiscal marls. The section is within the footwall of steep emergent thrust. Beds are almost horizontal all along the outcrop, except near the thrust where a footwall syncline developed. Therefore, this outcrop is a natural laboratory to monitor strain intensification within almost literally the same beds. The principal results are:

- ✓ Arro-Fiscal marls experienced a 160-200°C burial temperature, which resulted in dissolution of ferromagnetic particles and illite authigenis.
- ✓ The magnetic fabric is governed by illite all along the outcrop.
- ✓ In the cleavage-free domain (2 km from the thrust), the magnetic fabric is bedding-parallel, showing the development of magnetic lineations parallel to the fold axis.
- ✓ In the pencil cleavage domain (1 km to 0.2 km from thrust), the magnetic foliations remain parallel to bedding in average.
- ✓ In the slaty cleavage domain (<0.2 km from thrust), the magnetic foliation shifts toward the cleavage plane.
- ✓ The corrected degree of anisotropy is decreasing regularly from cleavage-free domain to the slaty cleavage domain
- ✓ The shape parameter displays an oblate-prolate-path when approaching the thrust.
- ✓ A value of strain is derived from the eigen values of the magnetic fabrics, assuming rigid rotation of illite particles.
- ✓ This strain evolves as a power law when approaching the thrust
- ✓ Both the kilometric-extent of the strain halo and power-law are consistent with the trishear modeling of the thrust.

From a general perspective, the measurement of low-field magnetic anisotropy in shales that have been moderately buried allows a fast access to describe the bulk fabric of billions of grains. We show in this study that damage of the matrix can be monitored with a

great accuracy and sensitivity. Because shales are important economic rocks, this technique might be helpful to check about their matrix properties.

Acknowledgments

This work has been founded by a CARNOT Isifor grant and CDAPP region grant. TB acknowledge support from the Total Chair of Structural Geology at UPPA (JPC). We thank François Martin and Michel Thibaut of the University Paul Sabatier, Toulouse, for the XRD measurements. We thank C. Passchier and two anonymous reviewers for constructive and helpful reviews.

References

- Allmendinger, R.W., 1998. Inverse and forward numerical modeling of trishear fault-propagation folds. *Tectonics* 17, 640–656. <https://doi.org/doi:10.1029/98TC01907>
- Aubourg, C., Jackson, M., Ducoux, M., Mansour, M., 2019. Magnetite-out and pyrrhotite-in temperatures in shales and slates. *Terra Nov.* 1–6. <https://doi.org/10.1111/ter.12424>
- Aubourg, C., Pozzi, J.P., 2010. Toward a new <250°C pyrrhotite-magnetite geothermometer for claystones. *Earth Planet. Sci. Lett.* 294, 47–57. <https://doi.org/10.1016/j.epsl.2010.02.045>
- Aubourg, C., Smith, B., Bakhtari, H., Guya, N., Eshragi, A., Lallemand, S., Molinaro, M., Braud, X., Delaunay, S., 2004. Post-miocene shortening pictured by magnetic fabric across the Zagros-Makran syntaxis (Iran). *Spec. Pap. Geol. Soc. Am.* 383, 17–40. [https://doi.org/10.1130/0-8137-2383-3\(2004\)383\[17:PSPBMF\]2.0.CO;2](https://doi.org/10.1130/0-8137-2383-3(2004)383[17:PSPBMF]2.0.CO;2)
- Cardozo, N., Allmendinger, R.W., Morgan, J.K., 2005. Influence of mechanical stratigraphy and initial stress state on the formation of two fault propagation folds. *J. Struct. Geol.* 27, 1954–1972. <https://doi.org/10.1016/j.jsg.2005.06.003>
- Casas-Sainz, A.M., Gil-Imaz, A., Simón, J.L., Izquierdo-Llavall, E., Aldega, L., Román-Berdiel, T., Osácar, M.C., Pueyo-Anchuela, Ó., Ansón, M., García-Lasanta, C., Corrado, S., Invernizzi, C., Caricchi, C., 2018. Strain indicators and magnetic fabric in intraplate fault zones: Case study of Daroca thrust, Iberian Chain, Spain. *Tectonophysics* 730, 29–47. <https://doi.org/10.1016/j.tecto.2018.02.013>
- Cifelli, F., Mattei, M., Hirt, A.M., Günther, A., 2004. The origin of tectonic fabrics in “undeformed” clays: The early stages of deformation in extensional sedimentary basins. *Geophys. Res. Lett.* 31, 2–5. <https://doi.org/10.1029/2004GL019609>
- Crognier, N., Hoareau, G., Aubourg, C., Dubois, M., Lacroix, B., Branellec, M., Callot, J.P., Vennemann, T., 2018. Syn-orogenic fluid flow in the Jaca basin (south Pyrenean fold and thrust belt) from fracture and vein analyses. *Basin Res.* 30, 187–216. <https://doi.org/10.1111/bre.12249>
- Erslev, E.A., 1991. Trishear fault-propagation folding. *Geology* 19, 617–620. [https://doi.org/10.1130/0091-7613\(1991\)019<0617:TFFP>2.3.CO;2](https://doi.org/10.1130/0091-7613(1991)019<0617:TFFP>2.3.CO;2)

- Godec, M., Koperna, G., Petrusak, R., Oudinot, A., 2013. Potential for enhanced gas recovery and CO₂ storage in the Marcellus Shale in the Eastern United States. *Int. J. Coal Geol.* 118, 95–104.
<https://doi.org/https://doi.org/10.1016/j.coal.2013.05.007>
- Haines, S.H., van der Pluijm, B.A., Ikari, M.J., Saffer, D.M., Marone, C., 2009. Clay fabric intensity in natural and artificial fault gouges: Implications for brittle fault zone processes and sedimentary basin clay fabric evolution. *J. Geophys. Res. Solid Earth* 114. <https://doi.org/doi:10.1029/2008JB005866>
- Hardy, S., Allmendinger, R.W., 2011. Trishear: A review of kinematics, mechanics, and applications. *AAPG Mem.* 95–119. <https://doi.org/10.1306/13251334M943429>
- Hardy, S., Ford, M., 1997. Numerical modeling of trishear fault propagation folding. *Tectonics* 16, 841–854.
<https://doi.org/doi:10.1029/97TC01171>
- Hirt, A.M., Lowrie, W., Lüneburg, C., Lebit, H., Engelder, T., 2004. Magnetic and mineral fabric development in the Ordovician Martinsburg Formation in the Central Appalachian Fold and Thrust Belt, Pennsylvania. *Geol. Soc. Spec. Publ.* 238, 109–126. <https://doi.org/10.1144/GSL.SP.2004.238.01.09>
- Ho, N.-C., Peacor, D.R., van der Pluijm, B.A., 1995. Reorientation mechanisms of phyllosilicates in the mudstone-to-slate transition at Lehigh Gap, Pennsylvania. *J. Struct. Geol.* 17, 345–356.
[https://doi.org/https://doi.org/10.1016/0191-8141\(94\)00065-8](https://doi.org/https://doi.org/10.1016/0191-8141(94)00065-8)
- Holeywell, R.C., Tullis, T.E., 1975. Mineral reorientation and slaty cleavage in the Martinsburg formation, Lehigh Gap, Pennsylvania. *Bull. Geol. Soc. Am.* 86, 1296–1304. [https://doi.org/10.1130/0016-7606\(1975\)86<1296:MRASCI>2.0.CO;2](https://doi.org/10.1130/0016-7606(1975)86<1296:MRASCI>2.0.CO;2)
- Hooyer, T.S., Iverson, N.R., 2000. Clast-fabric development in a shearing granular material: Implications for subglacial till and fault gouge. *GSA Bull.* 112, 683–692. [https://doi.org/10.1130/0016-7606\(2000\)112<683:CDIASG>2.0.CO;2](https://doi.org/10.1130/0016-7606(2000)112<683:CDIASG>2.0.CO;2)
- Housen, B.A., van der Pluijm, B.A., 1990. Chlorite control of correlations between strain and anisotropy of magnetic susceptibility. *Phys. Earth Planet. Inter.* 61, 315–323.
[https://doi.org/https://doi.org/10.1016/0031-9201\(90\)90114-D](https://doi.org/https://doi.org/10.1016/0031-9201(90)90114-D)
- Housen, B.A., Van Der Pluijm, B.A., 1991. Slaty cleavage development and magnetic anisotropy fabrics. *J. Geophys. Res.* 96, 9937–9946. <https://doi.org/10.1029/91JB00605>
- Hrouda, F., Schulmann, K., Suppes, M., Ullemayer, K., de Wall, H., Weber, K., 1997. Quantitative relationship between low-field AMS and phyllosilicate fabric: A review. *Phys. Chem. Earth* 22, 153–156.
[https://doi.org/https://doi.org/10.1016/S0079-1946\(97\)00094-3](https://doi.org/https://doi.org/10.1016/S0079-1946(97)00094-3)
- Humbert, F., Louis, L., Robion, P., 2014. Method for estimating ductile horizontal strain from magnetic fabrics in poorly consolidated clay-rich sediments. *Tectonophysics* 629, 335–352.
<https://doi.org/10.1016/j.tecto.2014.07.003>
- Izquierdo-Llavall, E., Aldega, L., Cantarelli, V., Corrado, S., Gil-Peña, I., Invernizzi, C., Casas, A.M., 2013. On the origin of cleavage in the Central Pyrenees: Structural and paleo-thermal study. *Tectonophysics* 608, 303–318. <https://doi.org/10.1016/j.tecto.2013.09.027>
- Jelínek, V., Kropáček, V., 1978. Statistical processing of anisotropy of magnetic susceptibility measured on groups of specimens. *Stud. Geophys. Geod.* 22, 50–62. <https://doi.org/10.1007/BF01613632>

- Kars, M., Aubourg, C., Pozzi, J.P., 2011. Low temperature magnetic behaviour near 35 K in unmetamorphosed claystones. *Geophys. J. Int.* 186, 1029–1035. <https://doi.org/10.1111/j.1365-246X.2011.05121.x>
- Kars, M., Aubourg, C., Suárez-Ruiz, I., 2015. Neoformed magnetic minerals as an indicator of moderate burial: The key example of middle Paleozoic sedimentary rocks, West Virginia. *Am. Assoc. Pet. Geol. Bull.* 99, 389–401. <https://doi.org/10.1306/06301413006>
- KISCH, H.J., 1991. Development of slaty cleavage and degree of very-low-grade metamorphism: a review. *J. Metamorph. Geol.* 9, 735–750. <https://doi.org/10.1111/j.1525-1314.1991.tb00562.x>
- Labaume, P., Séguet, M., Seyve, C., 1985. Evolution of a turbiditic foreland basin and analogy with an accretionary prism: Example of the Eocene South-Pyrenean Basin. *Tectonics* 4, 661–685. <https://doi.org/doi:10.1029/TC004i007p00661>
- Lee, J.H., Peacor, D.R., Lewis, D.D., Wintsch, R.P., 1986. Evidence for syntectonic crystallization for the mudstone to slate transition at Lehigh gap, Pennsylvania, U.S.A. *J. Struct. Geol.* 8, 767–780. [https://doi.org/10.1016/0191-8141\(86\)90024-6](https://doi.org/10.1016/0191-8141(86)90024-6)
- Lee, J.H., Peacor, D.R., Lewis, D.D., Wintsch, R.P., 1984. Chlorite-illite/muscovite interlayered and interstratified crystals: A TEM/STEM study. *Contrib. to Mineral. Petrol.* 88, 372–385. <https://doi.org/10.1007/BF00376762>
- Ma, L., Slater, T., Dowey, P.J., Yue, S., Rutter, E.H., Taylor, K.G., Lee, P.D., 2018. Hierarchical integration of porosity in shales. *Sci. Rep.* 8, 1–14. <https://doi.org/10.1038/s41598-018-30153-x>
- March, A., 1932. Mathematical theory on regulation according to the particle shape in affine deformation. *Zeitschrift Fur Krist.* 81 (3/4), 285–297.
- Morley, C.K., von Hagke, C., Hansberry, R., Collins, A., Kanitpanyacharoen, W., King, R., 2018. Review of major shale-dominated detachment and thrust characteristics in the diagenetic zone: Part II, rock mechanics and microscopic scale. *Earth-Science Rev.* 176, 19–50. <https://doi.org/10.1016/j.earscirev.2017.09.015>
- Özdemir, Ö., Dunlop, D.J., Moskowitz, B.M., 1993. The effect of oxidation on the Verwey transition in magnetite. *Geophys. Res. Lett.* 20, 1671–1674. <https://doi.org/doi:10.1029/93GL01483>
- Parés, J.M., 2015. Sixty years of anisotropy of magnetic susceptibility in deformed sedimentary rocks. *Front. Earth Sci.* 3, 1–13. <https://doi.org/10.3389/feart.2015.00004>
- Parés, J.M., Van der Pluijm, B.A., Dinarès-Turell, J., 1999. Evolution of magnetic fabrics during incipient deformation of mudrocks (Pyrenees, northern Spain). *Tectonophysics* 307, 1–14. [https://doi.org/10.1016/S0040-1951\(99\)00115-8](https://doi.org/10.1016/S0040-1951(99)00115-8)
- Pueyo Anchuela, Ó., Gil Imaz, A., Pocoví Juan, A., 2010. Significance of AMS in multilayer systems in fold-and-thrust belts. A case study from the Eocene turbidites in the Southern Pyrenees (Spain). *Geol. J.* 45, 544–561. <https://doi.org/10.1002/gj.1194>
- Puigdefàbregas, C., 1975. La sedimentación molásica en la cuenca de Jaca.
- Robion, P., Grelaud, S., Frizon de Lamotte, D., 2007. Pre-folding magnetic fabrics in fold-and-thrust belts: Why the apparent internal deformation of the sedimentary rocks from the Minervois basin (NE - Pyrenees, France) is so high compared to the Potwar basin (SW - Himalaya, Pakistan)? *Sediment. Geol.* 196, 181–200. <https://doi.org/10.1016/j.sedgeo.2006.08.007>
- Rochette, P., Jackson, M., Aubourg, C., 1992. Rock magnetism and the interpretation of anisotropy of magnetic

- susceptibility. *Rev. Geophys.* 30, 209–226. <https://doi.org/doi:10.1029/92RG00733>
- Teixell, A., 1996. The Ansó transect of the southern Pyrenees: Basement and cover thrust geometries. *J. Geol. Soc. London.* 153, 301–310. <https://doi.org/10.1144/gsjgs.153.2.0301>
- Thury, M., Bossart, P., 1999. The Mont Terri rock laboratory, a new international research project in a Mesozoic shale formation, in Switzerland. *Eng. Geol.* 59, 347–359. [https://doi.org/10.1016/s0013-7952\(99\)00015-0](https://doi.org/10.1016/s0013-7952(99)00015-0)
- van der Pluijm, B.A., Ho, N.-C., Peacor, D.R., Merriman, R.J., 1998. Contradictions of slate formation resolved? *Nature* 392, 348. <https://doi.org/10.1038/32810>
- Weil, A.B., Yonkee, W.A., 2012. Layer-parallel shortening across the Sevier fold-thrust belt and Laramide foreland of Wyoming: Spatial and temporal evolution of a complex geodynamic system. *Earth Planet. Sci. Lett.* 357–358, 405–420. <https://doi.org/10.1016/j.epsl.2012.09.021>
- Wenk, H.R., Kanitpanyacharoen, W., Ren, Y., 2019. Slate – A new record for crystal preferred orientation. *J. Struct. Geol.* 125, 319–324. <https://doi.org/10.1016/j.jsg.2017.12.009>
- Wenk, H.R., Voltolini, M., Kern, H., Popp, T., Mazurek, M., 2008. Anisotropy in shale from Mont Terri. *Lead. Edge (Tulsa, OK)* 27, 742–748. <https://doi.org/10.1190/1.2944158>
- Zehnder, A.T., Allmendinger, R.W., 2000. Velocity field for the trishear model. *J. Struct. Geol.* 22, 1009–1014. [https://doi.org/https://doi.org/10.1016/S0191-8141\(00\)00037-7](https://doi.org/https://doi.org/10.1016/S0191-8141(00)00037-7)

Figure captions

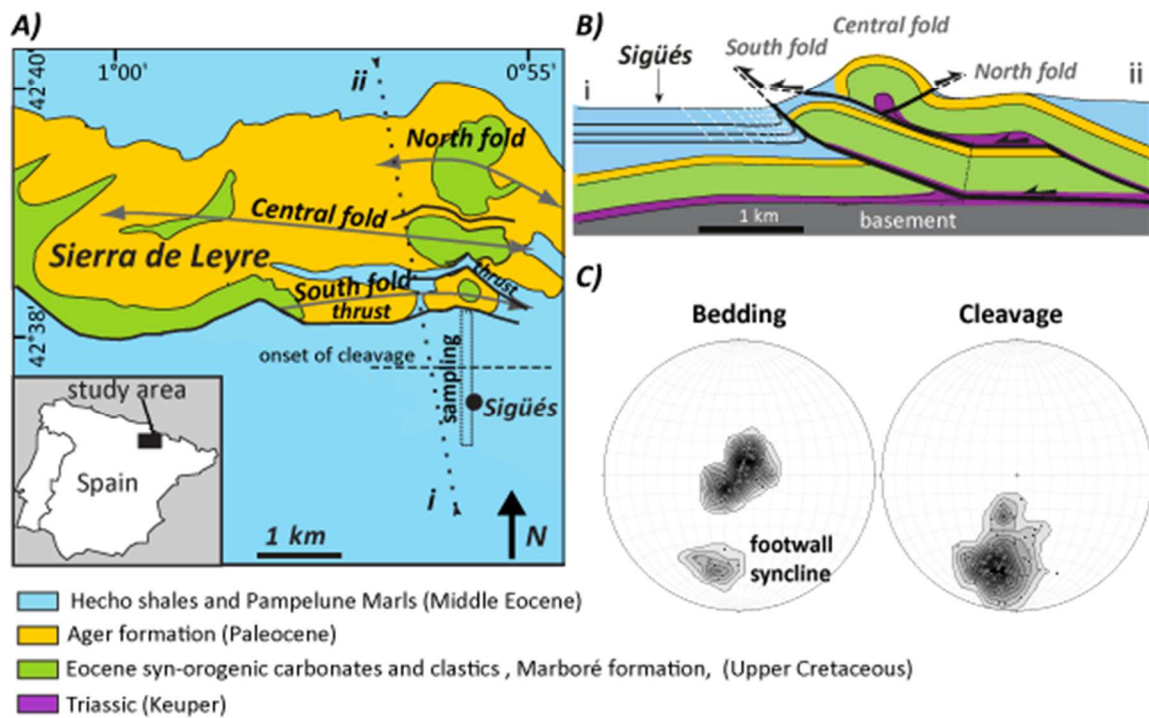


Figure 1. A) Simplified geological map, modified from Puigdefàbregas (1975). The footwall of the South Fold thrust developed a km-large damage zone. Pencil structures and incipient pencil cleavage developed at 1 km south of emergent thrust. B) Cross-section, modified from Labaume et al. (1985). Eocene Hecho shales (Arro-Fiscal Fm.) are not differentiated from the Pampelune shales. Bedding (black lines) and cleavage (white dashed lines) are indicated within Hecho Shales. C) Contour plot of poles of bedding and cleavage all along studied outcrop. Note that the bedding is sub-horizontal except near the thrust where a footwall syncline developed.

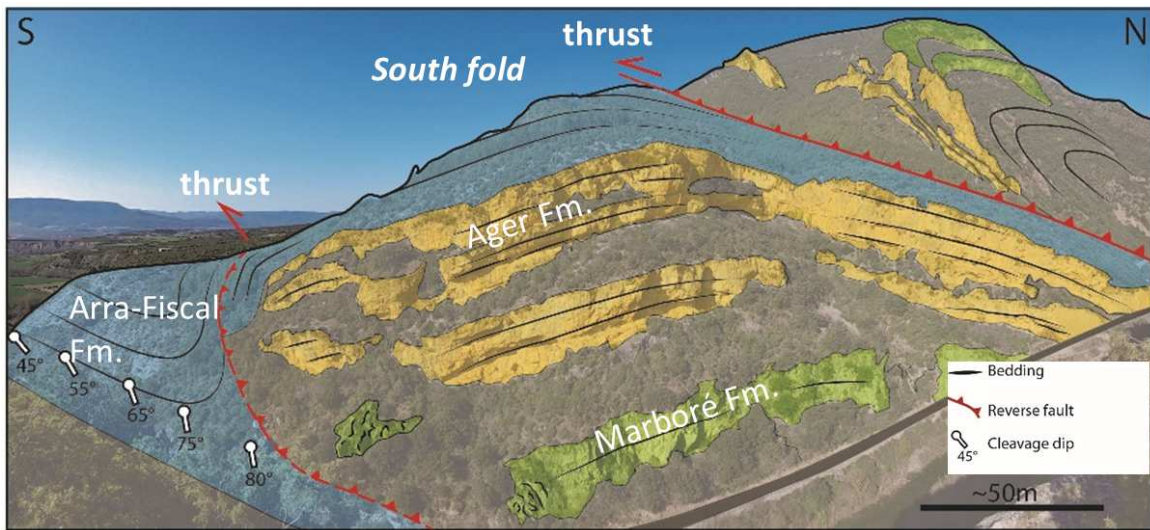


Figure 2. Interpreted photo of the western flank of the South Fold and Central fold. Note the abrupt termination of Ager Fm. against the Eocene shales (Arro-Fiscal Marls). Dip of cleavage is indicated (white pin line).

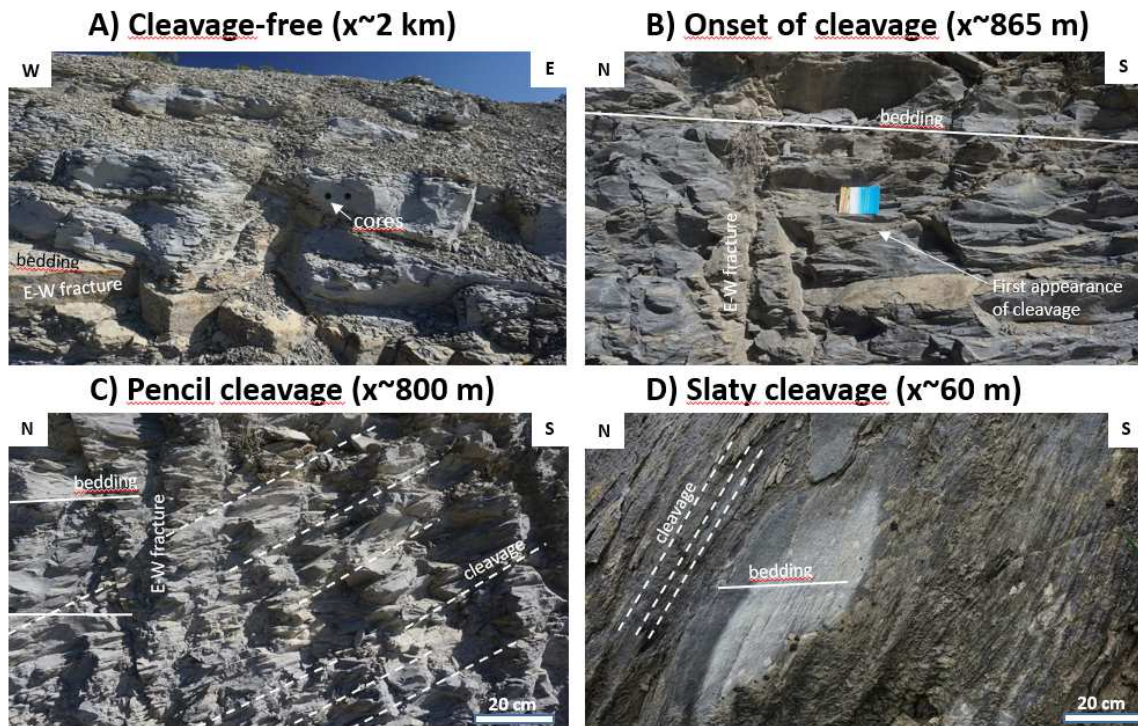


Figure 3 Outcrop photos. Bedding is almost horizontal. A) Only bedding and fracture network is observed in the Hecho Marls. Core of 25 mm diameter provides the scale. B) Discrete planes dipping to the North marked the onset of pencil cleavage. C) Large development of pencil cleavage. D) Steep cleavage, which almost superimposes the bedding.

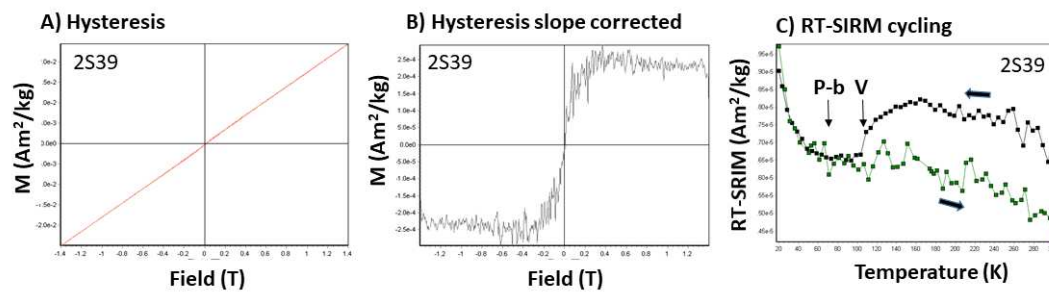


Figure 4 A) Hysteresis loop of representative specimens (sample 2S39). B) Hysteresis loop after slope correction. C) Low temperature investigation of artificial remanence. V : Verwey transition, which is diagnostic of magnetite. P-b: P-behavior, which is correlated to superparamagnetic grains. M : induced magnetization. RT-SIRM: room temperature saturated remanent magnetization.

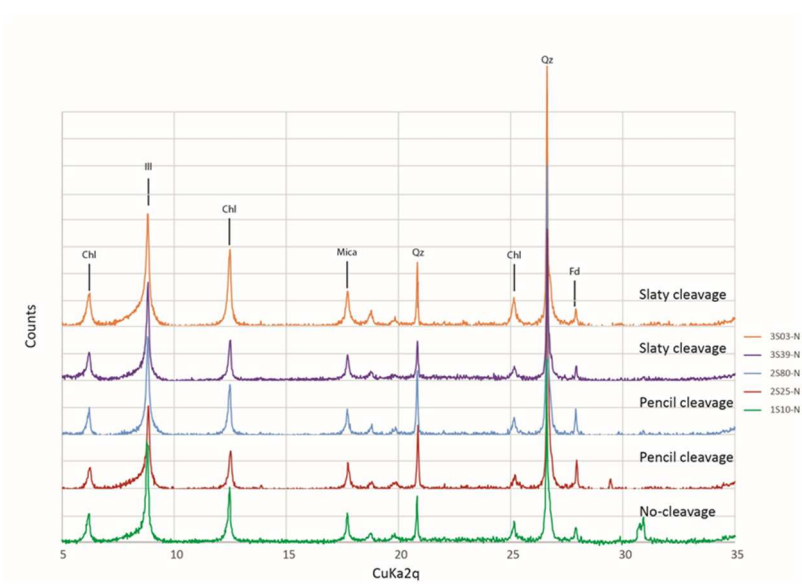


Figure 5 XRD Spectra. Chl = Chlorite, Ill = Illite, Qz = Quartz, Fd = Feldspar.

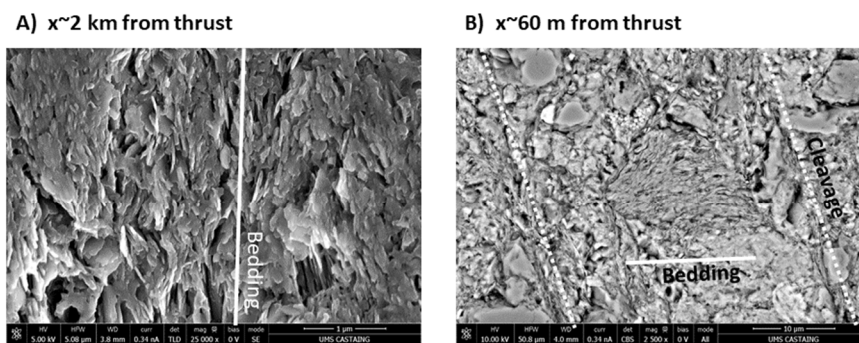


Figure 6 Scanning Electron Microscope (backscattered). A) No-cleavage sample. Clays (mostly illite) are aligned parallel to bedding. B) Slaty cleavage sample. Clays display different patches of organization. Some are parallel to cleavage. Others, parallel to bedding.

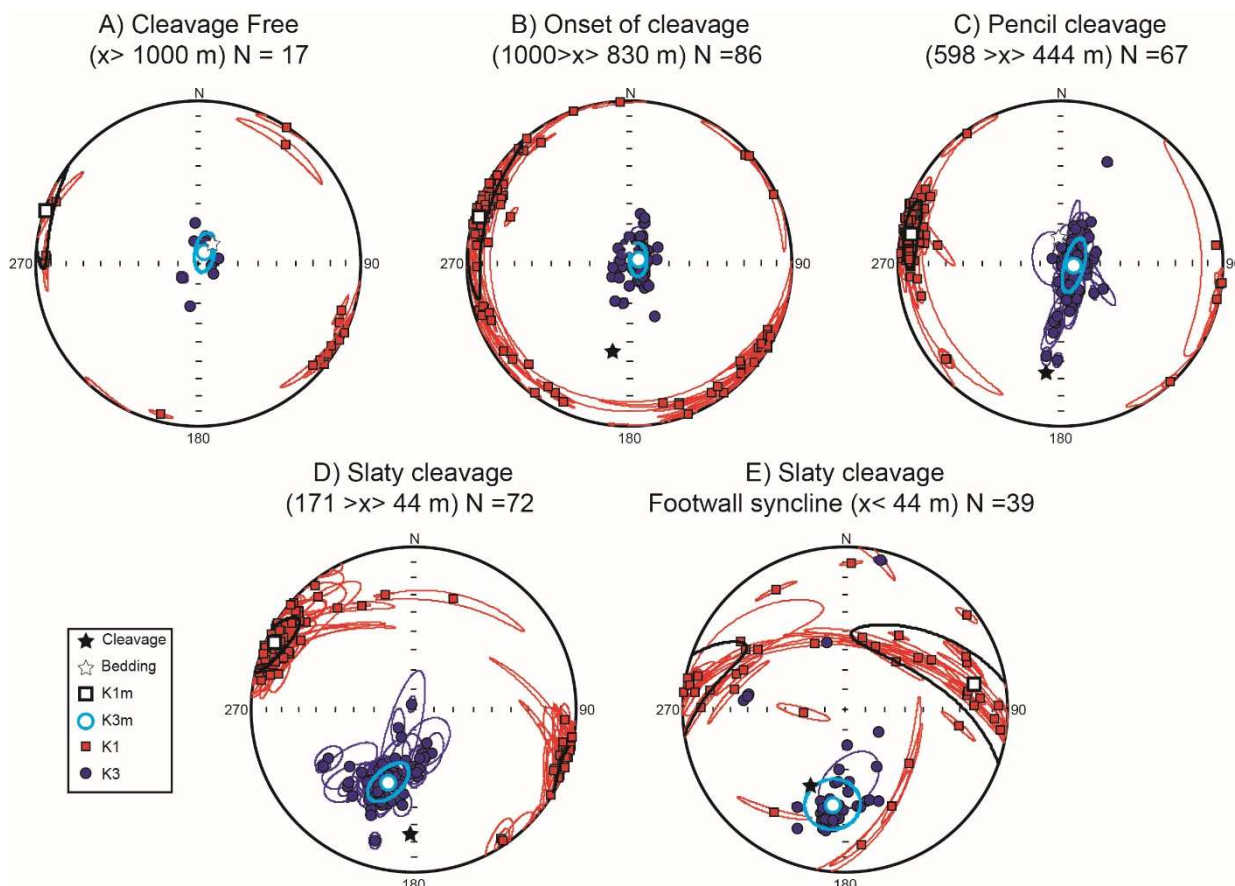


Figure 7 Stereoplots of AMS in geographic coordinates. K1 and K3 are plotted with their respective confidence angles at 95%. Mean K1m and K3m are obtained from tensorial mean and their respective

confidence angles at 95 % in light blue and black. Pole of cleavages (black star) and beddings (white star) are indicated.

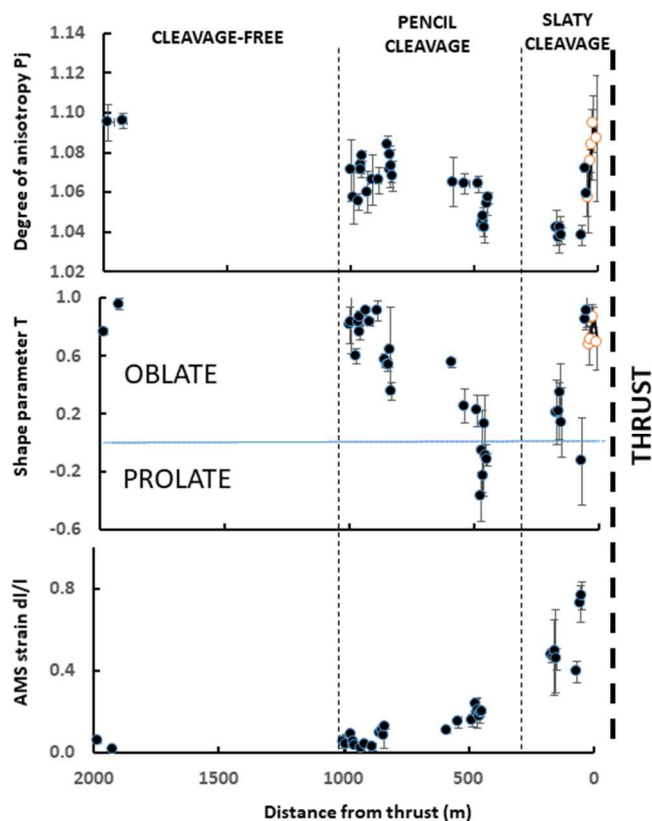


Figure 8 Scalar AMS data versus distance of the thrust (right of the diagram). A) Degree of anisotropy P_j , B) shape parameter T . C) strain d/l calculated from eigen values of AMS. Open symbols correspond to footwall syncline samples.

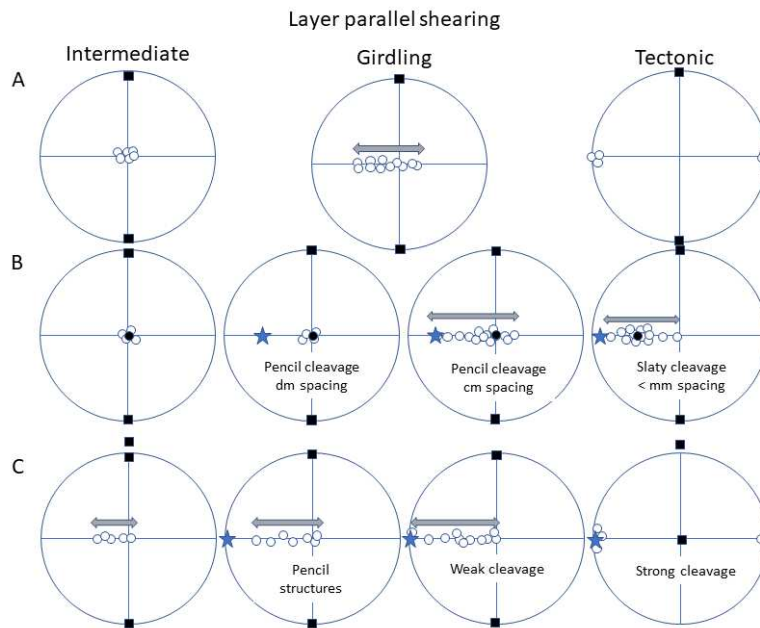


Figure 9 Schematic sketch of AMS data during layer parallel shearing. Open symbols are individual samples (circle = K3, square = K1). Black squares and circles symbols refers to average. Blue star refers to pole of cleavage. Grey double arrow represents approximate extent of girdle. Sigüés and Lehigh gap data are schematized. A) Parés (2015) 3-step evolution. B) This Study. Sigüés 4-step evolution. C) Lehigh-Gap 4-step evolution according to Hirt et al. (2004). No mean tensor was available from this study. Note that in B and C, the bedding has been restored to the horizontal, and stereoplots rotated, to fit with idealized top-to-the-left shear.

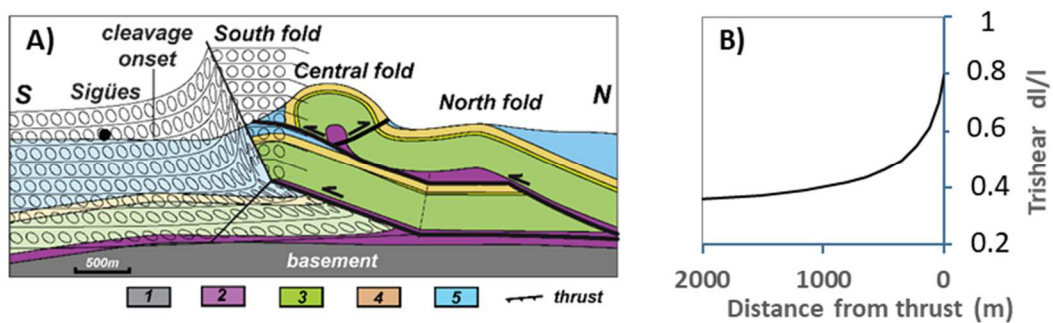


Figure 10 A) Trishear model applied to Sigüés South fold. Apical angle 110° . P/S ratio = 1, which indicates that the thrust propagates (P) at the same rate that shortening (S) (caption: 1: Basement rocks; 2: Trias; 3: Marboré Fm., upper Cretaceous; 4: Ager Fm.; 5: Arro Fiscal Marls). Shortening 1.5 km. B) Computed strain along horizontal line from the emerged thrust (the right part of the triangle zone), parallel to the topography.